Cooling of High-Energy Hadron Beams

Michael Blaskiewicz

Brookhaven National Laboratory, Upton, New York 11973; email: blaskiewicz@bnl.gov

Annu. Rev. Nucl. Part. Sci. 2014. 64:299–317

First published online as a Review in Advance on July 2, 2014

The *Annual Review of Nuclear and Particle Science* is online at nucl.annualreviews.org

This article's doi: 10.1146/annurev-nucl-102313-025427

Keywords

collider, stochastic cooling, electron cooling

Abstract

In this article, I discuss existing and planned techniques for cooling high-energy hadron beams, provide practical formulae for estimating cooling rates, and address difficulties and challenges.

Contents

1. INTRODUCTION

Data-acquisition sessions in hadron colliders typically last several hours. During this time, the number of particles in the beam drops due to burn-off from collisions and other losses. Concurrently, the beam size, characterized by its phase-space volume or emittance, usually increases due to various noiselike processes. Both of these effects cause the collision rate to decrease. Beam cooling addresses the problem of emittance growth, resulting in constant, and even decreasing, emittance. Proven methods of beam cooling are microwave stochastic cooling and electron cooling, which are well-tested technologies at low energy. Microwave stochastic cooling has been used at 100 GeV nucleon^{-1} energies but is limited to $\sim 10^9$ particles per bunch. Given the necessary event rates, this number of particles limits stochastic cooling to medium- and heavy-ion beams. Electron cooling works at high beam currents and has been used for proton energies up to 8 GeV, but cooling schemes for 100 GeV nucleon^{-1} gold and even 150 GeV protons have been designed. Optical stochastic cooling and coherent electron cooling can be viewed as high-bandwidth versions of microwave stochastic cooling. These new techniques hold promise for cooling proton beams at high energy. This review lists the sources of emittance growth and discusses the four cooling techniques in turn.

2. EMITTANCE GROWTH

Emittance growth in collider beams can arise from environmental noise or intrinsic processes and is usually due to both. Environmental noise can creep in through the radio-frequency (RF) accelerating system due to phase noise in the clocks driving the system. Tune ripple due to 50–60 Hz harmonics in the power supplies cause slow emittance growth. Mechanical oscillations of magnets have been observed in the Relativistic Heavy-Ion Collider (RHIC), causing 10 Hz oscillations in the closed orbit, thereby limiting performance. Intrinsic sources of emittance growth include intrabeam scattering (IBS), long-range Coulomb scattering, and dynamic emittance growth from lattice imperfections and the beam–beam force.

IBS results from multiple small-angle scattering between the ions within a bunch (1). When all effects are included, the equations for IBS become quite involved (2, pp. 155–59). However, the main ideas (3) are straightforward. During acceleration, the longitudinal phase-space volume $\Delta p_z \Delta z$ is roughly conserved, which holds for the other dimensions as well. For fixed RF voltage, the bunch length in the lab frame drops with increasing relativistic γ as $\gamma^{-1/4}$, so the rest frame bunch length increases as $\gamma^{3/4}$ and the rest frame longitudinal momentum spread decreases as $\gamma^{-3/4}$. The transverse focal length does not change with energy, so the ratio of the transverse beam size to the spread in transverse angles does not change with energy. Because $\Delta x \Delta p_x$ is conserved, Δp_x increases as $\gamma^{1/2}$, and one ends up with transverse temperatures that are much higher than the longitudinal temperature. Thus, multiple scattering during the store heats the longitudinal dimension.

Horizontal emittance is influenced via dispersion, the variation of closed orbit with fractional energy error. When two particles collide, giving a large longitudinal momentum transfer, their equilibrium orbits shift horizontally, heating the horizontal dimension. Various errors and coupling usually end up transferring some of this heat to the vertical direction as well.

During the collision process, long-range Coulomb scattering leads to transverse emittance growth, and the beam–beam force effectively limits the smallest beam emittance allowed. Beam cooling allows us to combat and even overcome the diffusive processes allowing continuous operation near the beam–beam limit. Below, we discuss the various cooling techniques.

3. MICROWAVE STOCHASTIC COOLING

3.1. General Principles

A stochastic cooling system is a wide-band feedback loop (4, 5). **Figure 1** depicts the physical layout of a cooling system. The beam signal is sampled by the pickup. The beam and signal propagate from the pickup to the kicker, and a kick derived from the pickup signal is given to the beam. To illustrate the basic principle, we first consider energy cooling of a coasting beam.

With system bandwidth W, one obtains the time resolution $\tau \sim 1/(2W)$. For a beam of particles with charge q and current I, the longitudinal cooling system measures the average energy error of samples containing $N_s = I\tau/q$ particles each turn. This signal is filtered, amplified, and applied to the beam. The energy deviation of a given particle after the kick is related to the value

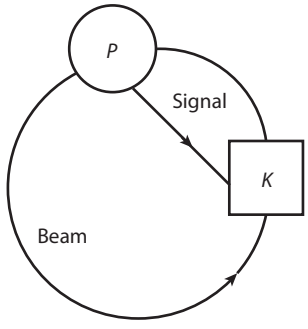

Figure 1

Schematic of a stochastic cooling system. A beam signal is sampled at the pickup (P) and sent to the kicker (K). Subsequently, upon arriving at the kicker, the beam receives a kick derived from the pickup signal.

before by

$$\bar{\epsilon}_j = \epsilon_j - \frac{g}{N_s} \sum_{k=1}^{N_s} \epsilon_k, \qquad 1.$$

where g is the system gain. Squaring both sides, assuming the ϵ_js are identically distributed, and averaging lead to

$$<\bar{\epsilon}^2> = <\epsilon^2> + \frac{g^2 - 2g}{N_s} \sum_{k=1}^{N_s} <\epsilon_j \epsilon_k>. \qquad 2.$$

Taking $<\epsilon_j \epsilon_k> = \sigma_\epsilon^2 \delta_{k,j}$, the optimal cooling rate corresponds to $g = 1$:

$$\frac{d\sigma_\epsilon^2}{dt} = -\frac{\sigma_\epsilon^2}{N_s T_{rev}}, \qquad 3.$$

where T_{rev} is the revolution period. Much of the hard work in stochastic cooling theory comes from evaluating the last term on the right-hand side of Equation 2. The decay of particle correlations leads to mixing (7) and depends on the detailed particle dynamics. If the beam requires M turns to mix the samples into statistical independence, then the optimal cooling time scales as $\sigma_\epsilon / \dot{\sigma}_\epsilon \approx 2 N_s T_{rev} M$.

Transverse pickups and kickers are used to reduce the transverse emittance. A transverse pickup measures the product of the beam current and beam offset, the dipole moment. The dipole signal is processed and sent to a kicker. The pickup and kicker locations are chosen so that offsets at the pickup propagate, via the magnetic lattice, to angles at the kicker. The kicker corrects the angle, reducing the emittance. After that, the argument is similar to the one for energy cooling. The resulting cooling rate is half of Equation 3 because the pickup measures only the position and the kick changes only the angle. In any case, these formulas are rules of thumb. For coasting beams, it is possible to obtain damped diffusion equations that are amenable to obtaining accurate solutions on a computer.

For high-energy hadron beams, there are always RF accelerating cavities operating that bunch the beam. Bunched beam stochastic cooling was observed in 1978 in the initial cooling experiment (ICE) (6). A theory of bunched beam cooling was developed in the early 1980s (8–10), and stochastic cooling systems for the SPS (11, 12) and the Tevatron (11, 13) were explored. For these colliders, the particle densities were much higher than those in ICE; early on (13–17), researchers found that RF activity extending up to very high frequencies made signal processing difficult. After much work, signal suppression was observed in the Tevatron (18). Cooling for heavy ions in RHIC (19, 20) was also considered and is now used as part of normal heavy-ion operations.

For N particles per bunch with a charge per particle of q, the power in coherent signals scales as $N^2 q^2$, whereas the power in Schottky signals scales as Nq^2. For a fixed charge per bunch, the relative power in Schottky versus coherent signals is proportional to the atomic number of the beam particles. Additionally, for the same charge per bunch one finds that IBS rates scale (roughly) as the atomic number, so density modulations in heavy-ion bunches diffuse more quickly than comparable modulations in proton bunches. Taken together, these findings suggest that the coherent line problem for heavy ions should be much less severe than it is for protons. This is indeed the case (21), and the signal processing for heavy ions is manageable.

As design of the RHIC cooling system proceeded, a new way of simulating stochastic cooling was found. The key to the algorithm is in Equation 3. If we decrease N_s by a factor of R, then the cooling rate increases by a factor of R. So, for a given fractional cooling, the number of simulation turns needed decreases by a factor of R and the number of particles tracked decreases by the same factor, yielding a net reduction factor of R^2 (22). It is important that the cooling and dynamical

timescales remain well separated, but values $R \sim 10^5$ are typical for both RHIC and the Large Hadron Collider (LHC). Typically, one needs 20,000 particles and tracks for a comparable number of turns. In this regime, it is possible to include IBS and position-dependent burn-off while doing the simulations on a midrange workstation (23).

As an example, consider longitudinal filter cooling (24). The first update takes the particles from just before the RF cavity over to the stochastic cooling pickup. For a particle n with charge q,

$$\bar{\epsilon}_n = \epsilon_n + q\, V_{\mathrm{RF}}(\tau_n), \qquad 4.$$

$$\bar{\tau}_n = \tau_n + \kappa_1 \bar{\epsilon}_n, \qquad 5.$$

where τ_n is the arrival time of particle n relative to the zero crossing of the RF voltage, $V_{\mathrm{RF}}(\tau_n)$ is the value of the RF voltage when the particle passes, ϵ_n is the energy deviation of the particle before crossing the cavity, and κ_1 is a constant that depends on the accelerator lattice and beam energy. When the particle arrives at the pickup, the instantaneous current of the beam is calculated on a uniform time grid of spacing Δt via

$$I(k\Delta t) = Q \sum_{j=1}^{N} \hat{\delta}(k\Delta t - \bar{\tau}_j), \qquad 6.$$

where the beam is represented by N macroparticles of charge $Q = Rq$. In the simplest case, $\hat{\delta}(t)$ is a triangle function of height $1/\Delta t$ and base $2\Delta t$.

Next, one transports the beam from the pickup to the kicker. The energy is unchanged, but the particle arrival time slips via $\bar{\bar{\tau}}_n = \bar{\tau}_n + \kappa_2 \bar{\epsilon}_n$, where κ_2/κ_1 is close to the ratio of the path lengths. The kick for simple filter cooling is driven by $\Delta I(k\Delta t) = I(k\Delta t) - I_{\mathrm{old}}(k\Delta t)$, where I_{old} was accumulated on the previous turn. This current creates a voltage via

$$V_s(\tau) = \int \mathrm{d}\tau_1 W(\tau_1) \Delta I(\tau - \tau_1), \qquad 7.$$

with

$$W(\tau) = 2 \int_{f_1}^{f_2} R(f) \sin(2\pi f \tau) \mathrm{d}f, \qquad 8.$$

where $R(f)$ is the frequency-dependent gain and the cooling frequency band is $[f_1, f_2]$. After the voltage is calculated, the kick is given to the beam as in Equation 4, and the process is repeated. Similar algorithms are employed for transverse cooling, and additional effects such as IBS and additive system noise are implemented using random processes. Betatron coupling, as well as burn-off due to collisions, has been included (25).

3.2. Implementation in RHIC and Possibilities for the LHC

Figure 2 depicts the RHIC cooling system, and **Table 1** provides the relevant parameters. We use one-turn delay filter cooling (24) for the longitudinal system. The two rings are similar, so we discuss the blue (clockwise) ring. The pickup is in the 2 o'clock straight section. This pickup signal is processed through a 16-branch traversal filter, giving

$$V_t(t) = \sum_{n=0}^{15} V_p(t - n\tau_0), \qquad 9.$$

where $\tau_0 = 5.000$ ns. The filter is constructed from coaxial cables without active components that could saturate. The signal is amplified and sent to the 4 o'clock receiver using an analog 70 GHz

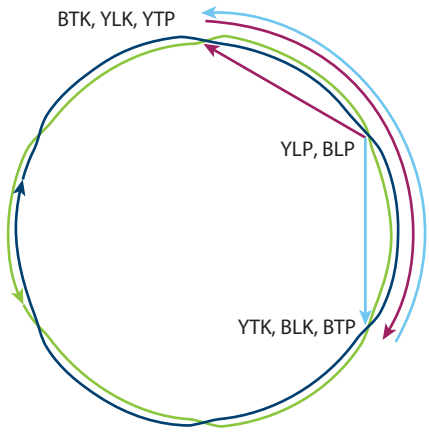

Figure 2

Schematic of the blue (*clockwise*) and yellow (*counterclockwise*) RHIC rings showing the locations of stochastic cooling components. The blue transverse kickers (BTK), yellow longitudinal kicker (YLK), and yellow transverse pickups (YTP) are in the 12 o'clock straight sections. The blue and yellow longitudinal pickups (BLP, YLP) are in the 2 o'clock straight sections. The yellow transverse kickers (YTK), blue longitudinal kicker (BLK), and blue transverse pickups (BTP) are in the 4 o'clock straight sections. The yellow beam path is in green; signal paths are in magenta. The blue beam path is in dark blue; signal paths are in light blue.

microwave link (26), resulting in a pickup-to-kicker delay of one-sixth of a turn. The signal then goes through a one-turn delay filter constructed from single-mode optical fiber. A key feature is that the modulation of the optical signal is accomplished via attenuation of the laser source, which reduces nonlinear effects. After the one-turn delay filter, the signal is split into 16 branches and the signals are passed through 100 MHz bandpass filters centered at 6.0, 6.2, . . . , 9.0 GHz. These signals first go through in-phase and quadrature (IQ) modulators that adjust the gain and phase, then go to 40 W solid-state amplifiers that power individual cavities. The cavities are split along the vertical plane and are open during injection and acceleration. After the beam reaches top energy, the cavities close down to a 2 cm aperture.

The transverse cooling system pickup plates were provided by Fermilab (27) and are moved with 5 μm precision translation stages. A difference signal is obtained, and a 16-stage traversal filter is applied. To prevent cross talk, the yellow (counterclockwise) ring uses frequencies of 4.8,

Table 1 RHIC parameters during the 2011 uranium run and proposed LHC lead parameters

Parameter	RHIC value	LHC value
Circumference	3,834 m	26,659 m
Betatron tunes	$Q_{x,y} = 28.22, 29.22$	$Q_{x,y} = 59.31, 64.32$
Transition γ	25.22	55.7
Beam energy	104 GeV nucleon^{-1}	2,786 GeV nucleon^{-1}
Ions per bunch	2.3×10^8	1.4×10^8
$h = 2{,}520$ voltage	2.8 MV	NA
$h = 360$ voltage	0.30 MV	NA
$h = 35{,}640$ voltage	NA	16 MV
Initial, normalized rms emittance	2.3 μm	1.43 μm

Abbreviations: NA, not applicable; rms, root mean square.

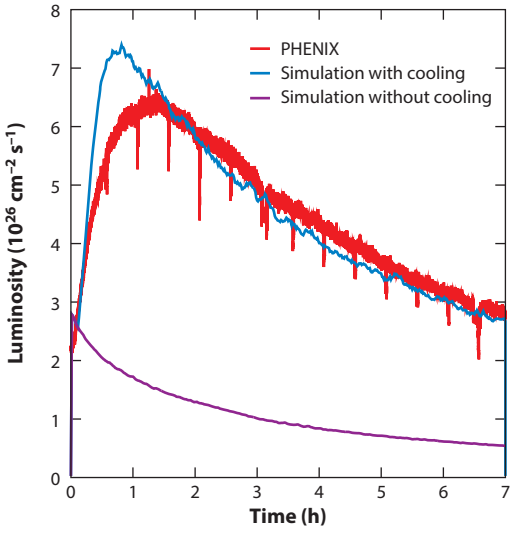

Figure 3

U + U luminosity versus time in RHIC as measured with the PHENIX detector and simulated with and without cooling. The periodic downward spikes occur during episodes of beam steering.

5.0, . . . , 7.8 GHz, whereas the blue ring uses 4.7, 4.9, . . . , 7.7 GHz. The latter is obtained by inserting -1^n in Equation 9. The signals are sent to their kickers via an optical fiber going in the opposite direction to the beam. The resulting net beam delay is two-thirds of a turn. The kicker cavities are similar to the longitudinal cavities except that we drive a transverse mode.

During operation, the 96 independent cavity systems are computer controlled. One cavity at a time, transfer switches insert a network analyzer into the signal path. The open-loop transfer function is measured and compared with a reference that had good cooling. The IQ modulators are adjusted to make the live transfer function as close to the stored one as possible. In this way, we step though all the cavities at startup, and approximately every 15 min hence, to accommodate system drifts and changes in the beam. **Figure 3** compares data and simulations for the effect of simultaneous longitudinal and transverse stochastic cooling of both beams on the luminosity for U + U collisions at one of the two large RHIC detectors. Cooling increases the time-integrated luminosity by a factor of approximately five.

A stochastic cooling system is under consideration to improve the heavy-ion luminosity in the LHC (28). We consider a 5–15 GHz system and a 5–20 GHz system with a frequency spacing of 1 GHz (11 or 16 cavities). The longitudinal gain is chosen to keep the cavity voltage mostly below 1 kV. **Figure 4** shows simulation results with one interaction point for 360 bunches of 1.4×10^8 lead ions per ring. Clearly, even with 11 cavities a significant gain is possible.

4. ELECTRON COOLING

4.1. General Principles

The basic idea of electron cooling is to introduce cold electrons into hot ions, cooling the ions (29–31). A cold electron beam with the same average velocity as the ion beam is generated. The electrons are much lighter, and a magnet is used to bend the electrons so that their beam trajectory coincides with that of the ions. Calculations are done in the comoving frame, where velocities are

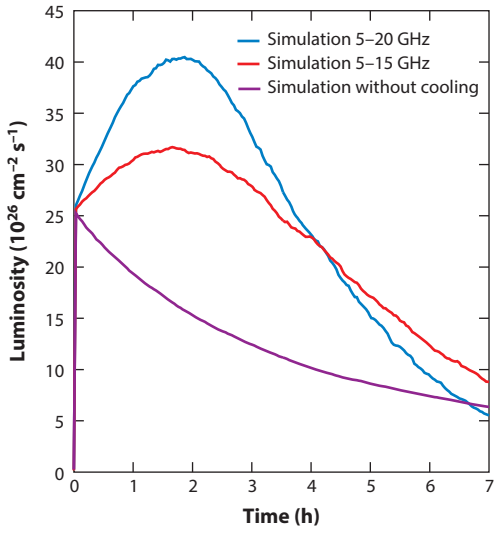

Figure 4

Pb + Pb luminosity versus time in the LHC simulated with and without cooling.

nonrelativistic. If the guiding fields are small, then the electron–ion collisions are well described by the Rutherford formula. The friction force on an ion is calculated using first-order perturbation theory (30–33):

$$\mathbf{F}(\mathbf{V}) = \frac{e^4 Z^2}{4\pi\epsilon_0^2 m} \int L \frac{\mathbf{v}-\mathbf{V}}{|\mathbf{v}-\mathbf{V}|^3} f_e(\mathbf{v}) \mathrm{d}^3 v, \qquad 10.$$

where Z is the atomic number of the fully stripped ion; $\mathbf{V}$ is the ion velocity; $f_e(\mathbf{v})\mathrm{d}^3 v$ is the number of electrons per unit volume in $\mathrm{d}^3 v$; e and m are the electron charge and mass, respectively; and $L = \ln(b_{\max}/b_{\min})$ is the Coulomb logarithm with impact parameter b. For high energies, the electron velocity distribution is usually flattened with longitudinal spread (along the beam direction) much smaller than the transverse spread. Even though the transverse emittance is large relative to the longitudinal, the absolute angular spread can be quite small, and several complications are involved in transporting the electron beam (34).

If the solenoidal magnetic field in the cooling section is large enough that the electron Larmor radii are significantly smaller than the beam radius, cooling can be significantly enhanced above that predicted by Equation 10. In particular, electron–ion collisions that occur over many Larmor oscillations and at distances larger than the Larmor radius are insensitive to the transverse velocity of the electrons (33). However, any deviations in the direction of the guiding solenoid field manifest themselves as if they were transverse velocities, which can easily offset the gain due to strong focusing.

Equation 10 has been tested against simulations (37). When the electron beam velocity spread is larger than the ion beam velocity spread, the emittance cooling rates are (2, pp. 202–5)

$$\begin{aligned} \lambda_{\parallel} &= 4\sqrt{\frac{2}{\pi}}\eta L \frac{n_e}{a^2} \frac{c r_e r_c}{\beta\theta_e^2 \gamma^3 \sigma(\gamma_e)}, \\ \lambda_{\perp} &= \sqrt{2\pi}\eta L \frac{n_e}{a^2} \frac{c r_e r_c}{\beta\theta_e^3 \gamma^5}, \end{aligned} \qquad 11.$$

where we are now in the lab frame. The classical radii of the ion and the electron are r_c and r_e, respectively; γ is the Lorentz factor; $\beta = v/c$; n_e is the line density of electrons in the lab frame;

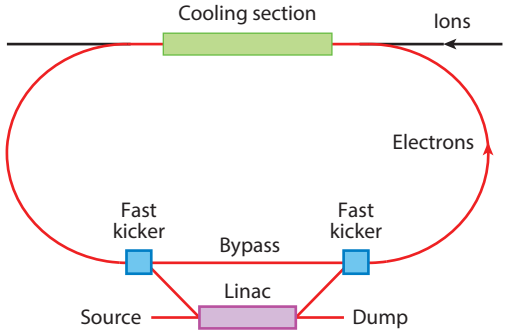

Figure 5

Schematic of the JLab electron cooler. The BNL design was similar but without the fast kicker and bypass. A single cooling section is shown, but both labs planned to use the same electron beam to cool both collider rings. Abbreviation: linac, linear accelerator. Modified from Reference 44.

c is the speed of light; η is the fraction of the ring occupied by the cooling solenoid; θ_e is the root-mean-square (rms) angular divergence of the electron beam in the cooling section; a is the electron beam radius; and $\sigma(\gamma_e)$ is the rms spread in the electron Lorentz factor. Equation 11 is only for rough estimates. Actual calculations require numerical integration that incorporates details of the phase-space distribution and includes heating effects such as IBS (35). Even so, Equation 11 clearly shows that the cooling time increases strongly with γ and that heavy ions with large r_c are preferred.

4.2. Early Design for RHIC and Possibilities for the Electron–Ion Collider

The highest-energy electron cooling to date was implemented in the Fermilab recycler (34, 36). The 8.9 GeV antiproton beam was cooled using a recirculated dc electron beam. Although precise magnetized transport was critical, the cooling was unmagnetized. For energies of order 100 GeV nucleon^{-1}, dc accelerators are unavailable, and electron cooling using a beam from an RF linear accelerator (linac) has been extensively studied for RHIC at Brookhaven National Laboratory (BNL) (37–41). The BNL design for a heavy-ion cooler involved average electron currents of order 100 mA with electron energies of 54 MeV. These values necessitated an energy recovery linac in which the electron beam is accelerated, passes through the cooling section, and then decelerates through the linac. The initial design called for magnetized cooling, but the most advanced design assumed unmagnetized cooling (42). With the success of stochastic cooling, design efforts were shifted to future BNL projects.

The medium-energy Electron–Ion Collider (MEIC) proposed for Thomas Jefferson National Accelerator Facility (JLab) also uses a linac but plans on magnetized cooling (43–45). Cooling will be employed at several stages during acceleration, exploiting the γ dependence in Equation 11. At top energy during collisions, the IBS growth time is a few minutes, requiring vigorous cooling to counteract it. **Figure 5** depicts a schematic of the JLab cooling system. The fast kickers and the source are all periodic, with the same period. Electrons start at the source and go through the linac. The high-energy electrons exit the linac and are bent up to the fast kicker, which bends the bunch into the arc on the right. The electron bunch passes through the cooling section, interacting with an ion bunch, and goes down the arc on the left. The fast kicker on the left is timed so that the electron bunch is not kicked and goes through the bypass. The kicker on the right is likewise timed, sending the electrons through the cooling section again. It is envisioned that the electrons

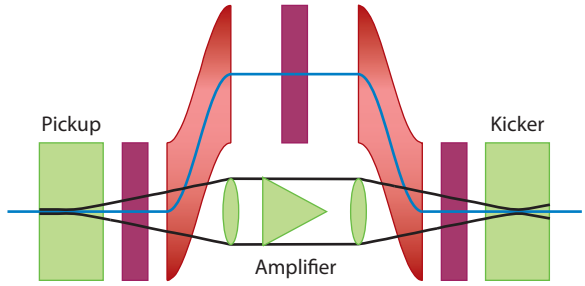

Figure 6

Schematic of optical stochastic cooling. Beams travel to the right; the optical envelope (*black*) corresponds to a 10-m-long kicker with $\lambda = 2$ μm and $Z_r = 1.57$ m. Magnetic elements are outlined in magenta and blue, and optical elements are outlined in green.

will circulate for $N_{\rm circ} \simeq 100$ turns before encountering a pulse from the fast kicker on the left. After that, the electrons are decelerated through the linac and dumped. In this way, the average electron current in the cooling section is a factor of $N_{\rm circ}$ greater than the average current in the acceleration section, greatly reducing stresses on the source, linac, and dump. The trade-off is that the fast kickers must be extremely stable and precise. Even with such an inspired design, the proton beam energy is limited to 150 GeV. Below, we consider techniques designed to cool high-intensity, high-energy proton beams.

5. OPTICAL STOCHASTIC COOLING

5.1. General Principles

Optical stochastic cooling (**Figure 6**) has been proposed to utilize the large absolute bandwidth of laser amplifiers (46–48), which can be 1,000 times the bandwidth of microwave systems. Initially, the ion beam passes through the wiggler pickup. For a planar wiggler with magnetic field $B_y = B_0 \cos(k_w s)$, the ions are given a transverse velocity $v_x = -{\rm c}K \sin(k_w s)/\gamma$; here, the wiggler parameter (in MKS units) is $K = Ze\,B_0/k_w M{\rm c}$, where M is the ion mass. Light is emitted with wavenumber (e.g., 49):

$$k = k_w \frac{2\gamma^2}{1 + K^2/2}. \qquad 12.$$

The light goes through the optical amplifier while the beam goes around a magnetic bypass, which we assume is in the horizontal plane. Consider a particle in the pickup with longitudinal coordinate $s_{\rm PU}$, which has coordinates x and x', and $\delta = (p - p_0)/p_0$. After traversing the bypass, the particle has the relative longitudinal position $\Delta z = {\rm c}(t_0 - t) = M_{5,1}x + M_{5,2}x' + M_{5,6}\delta$, where t and t_0 are, respectively, the times required for the particle and for a reference particle with $x = x' = \delta = 0$ to traverse the bypass. The transfer matrix elements, M_{ij}, correspond to partial derivatives of final values (i) with respect to initial values (j). Now consider the light pulse generated by the particle in the pickup wiggler. The initial pulse has a number of wavelengths equal to the number of wiggler periods. The pulse is amplified, band-limited, and focused by the optical system so that it gives a kick to the returning beam, $\Delta\delta = \kappa(\Delta z)\sin(k\Delta z)$, where the width is determined by the pickup pulse and the bandwidth of the amplifier. For small Δz the kick is linear in the coordinates, and the cooling rate for a single particle can be calculated in perturbation theory (48). For envisioned collider designs, this is an adequate approximation because the cooling is power limited. The

betatron and synchrotron amplitudes vary, respectively, as (48)

$$\frac{\mathrm{d}\ln\hat{x}_\beta}{\mathrm{d}n} = k\kappa_0\frac{M_{5,6}-\bar{\eta}}{2}, \qquad 13.$$

$$\frac{\mathrm{d}\ln\hat{\delta}}{\mathrm{d}n} = \frac{k\kappa_0\bar{\eta}}{2}, \qquad 14.$$

where n is the turn number and $\kappa_0 = \max\{\kappa(z)\}$. For ultrarelativistic beams, these parameters are related to the lattice functions by

$$\bar{\eta} = -\int_{s_{\mathrm{PU}}}^{s_{\mathrm{K}}}\frac{D(s)}{\rho(s)}\mathrm{d}s, \qquad 15.$$

where s_{K} is the kicker location, $D(s)$ is the periodic (usual) machine dispersion, and $\rho(s)$ is the orbital curvature. The other parameter is

$$M_{5,6} = -\int_{s_{\mathrm{PU}}}^{s_{\mathrm{K}}}\frac{D_0(s)}{\rho(s)}\mathrm{d}s, \qquad 16.$$

where D_0 is the solution of the dispersion equation with $D_0(s_{\mathrm{PU}}) = D_0'(s_{\mathrm{PU}}) = 0$. Transverse cooling requires nonzero dispersion (or its derivative) at the pickup and the kicker.

To estimate the kicker properties, we model the light as a Gaussian beam. From the parabolic wave equation, the transverse electric field is (50)

$$E_x = \frac{E_0 s_{\mathrm{R}}}{s_{\mathrm{R}}+is}\exp\left[\frac{-k(x^2+y^2)}{2(s_{\mathrm{R}}+is)}+ik(s-\mathrm{c}t)\right], \qquad 17.$$

where E_0 is the field at the waist and s_{R} is the Raleigh range. The particle to be kicked copropagates with the light in the undulator. Assuming phases are optimized, the light waist is centered in the kicker, and transverse amplitudes are small, the maximum kick is given by

$$\kappa_0 = \Delta\delta_{\max} = K\frac{qE_0 s_{\mathrm{R}}}{\gamma^2 Mc^2}\ln\left[\frac{L}{2s_{\mathrm{R}}}+\sqrt{1+\frac{L^2}{4s_{\mathrm{R}}^2}}\right], \qquad 18.$$

where L is the length of the wiggler. The power in the kicker depends on the bandwidth and beam current:

$$P = \sqrt{\frac{\pi}{2}}\frac{I}{q}\frac{s_{\mathrm{R}}E_0^2}{k\sigma_\omega Z_0}, \qquad 19.$$

where I is the beam current, σ_ω is the rms power bandwidth, and $Z_0 = 377\Omega$. In Equation 19 one may take I to be either the average current, which gives the average power, or the instantaneous current, which gives peak power and duty cycle. As with stochastic cooling, there is a limit to the cooling rate associated with the finite bandwidth and the other particles in the bunch. The mean-square average kick in δ is $<\delta^2> \approx \kappa_0^2 I/(q\sigma_\omega\sqrt{8\pi})$, where I is the instantaneous current at the test particle.

The transverse variables are influenced via the dispersion and its derivative at the kicker. Because the betatron cooling is purely horizontal, one can use betatron coupling to cool the vertical plane. In addition to the techniques mentioned above, enhanced optical cooling has been proposed (51, 52). By including a screen in the optical image plane, particles with a single sign of x are emphasized, and significant gains in cooling rate have been reported.

5.2. Possibilities for RHIC and the LHC

Optical stochastic cooling systems for RHIC (53), the Tevatron (48), and the LHC (54) have been proposed. Additionally, tests using electron rings have been proposed (55, 56). Construction of the

wigglers, optical system, and bypass involves challenges. Ti:sapphire lasers operate in the range between 0.65 and 1.1 μm (57), whereas optical parametric amplifiers can operate up to 12 μm (58). The parameter range of interest for cooling proton beams involves pulse lengths on the order of nanoseconds—very far from the timescales of interest for atomic experiments. Compromise needs to be reached on the simultaneous demands of high gain, wide bandwidth, short delay, and high power. The bypass for the beam must have $M_{5,6} \sim 1/[k\sigma(\delta)]$ stable at the $\lambda/8$ level and needs to have enough delay to compensate the optical delay through the lasing medium and any focusing elements. Note that $M_{5,6} = (s_K - s_{PU})/\gamma^2$ purely from the spread in beam velocity, which can be very significant for RHIC energies. The transport between the pickup and the kicker needs to be well behaved over the momentum spread of the beam.

Designs for these systems involve varying degrees of detail. The original RHIC application considered heavy ions, whereas current cooling efforts are focused on protons. An additional complication is that RHIC operates over a wide range of energies. Equation 12 reveals that either the frequency of the light changes or the wiggler needs to change. Light amplifiers have bandwidths $\lesssim$10%, so changing energies involves significant modifications of the cooling hardware. For the LHC, the energy is high enough that very little amplification may be needed (54).

6. COHERENT ELECTRON COOLING

6.1. General Principles

In 1992, Derbenev (59) proposed that electron beam instabilities could be used to enhance electron cooling. As of now, there are two primary methods. The first (**Figure 7**) involves a free electron laser (FEL) (60–66, 67) and the second a chicane (68). Electron bunches with the same speed as the ions are produced by a linac. A dipole magnet is used to merge the electron bunch with the ion bunch. The electrons shift to Debye-shield the ions. The electrons and ions are separated to allow for control of the ion optics. The electrons traverse a wiggler and undergo FEL instability while the ions traverse a bypass. The beams are recombined in the kicker section, and the space-charge fields from the electrons kick the ions. The optics are arranged so that these kicks cool the ion beam. Below, we examine the cooling process in more detail.

If we approximate the unperturbed electron distribution function in the rest frame to be

$$f_e(\mathbf{v}) = \frac{n_0}{\pi^2 v_\perp^2 v_z (1 + \mathbf{v}_\perp^2/w_\perp^2 + v_z^2/w_z^2)^2}, \qquad 20.$$

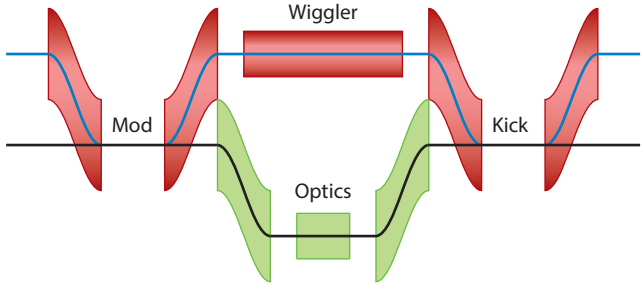

Figure 7

Schematic of coherent electron cooling. Beams travel to the right; electrons (*blue*) are affected by optical elements in the upper bypass between modulator and kicker sections, and hadrons (*black*) are affected primarily by optical elements in the lower bypass. Abbreviations: Kick, kicker; Mod, modulator.

then the perturbed electron charge density in the rest frame of an ion with relative velocity $\mathbf{V}$ satisfies (64)

$$\frac{\partial \rho_e(\mathbf{x}, t)}{\partial t} = -\frac{Ze\omega_p t \sin(\omega_p t)}{\pi^2 w_\perp^2 w_\parallel \left[t^2 + (\mathbf{x}_\perp - \mathbf{V}_\perp t)^2/w_\perp^2 + (z - V_z t)^2/w_z^2\right]^2}, \qquad 21.$$

where ω_p is the electron plasma frequency and Z is the atomic number of the ion that is introduced at $\mathbf{x} = 0$ and $t = 0$. The introduction is actually accomplished by merging the two beams by use of a bending magnet, but the process is short enough that approximating it by particle creation is adequate. Equation 21 agrees qualitatively with simulations using more realistic velocity distributions and within beams of bounded cross sections (69–72). If $V = 0$, then the charge density as $t \to \infty$ is

$$\rho_\infty(\mathbf{x}) = -Ze\frac{\exp(-\bar{r})}{4\pi r_\perp^2 r_z \bar{r}}, \qquad 22.$$

where $r_{\perp,z} = w_{\perp,z}/\omega_p$ and $\bar{r}^2 = \mathbf{x}_\perp^2/r_\perp^2 + z^2/r_z^2$. In an ideal application, the modulator section is on the order of one-half of a plasma oscillation long, and density perturbations similar to Equation 22 result. Magnetic chicanes have been invoked to create density modulations from momentum perturbations for more rigid electron beams (61). Integrating Equation 22 over the two transverse coordinates and accounting for Lorentz contraction yield a perturbed electron line density in the lab frame of $\delta n_0(z) = -\gamma Z \exp(-\gamma|z|/r_z)/2r_z$.

The electron beam is then bent out of the ion beam and sent through the FEL while the ions traverse a bypass. The current fluctuations in the electron beam are amplified by the FEL instability. In the linear approximation, each ion creates a seed for the FEL, as does each electron. Assuming $r_z/\gamma \ll \lambda$, the ion and electron perturbations are amplified by the same Green function. Let $\delta n_\ell(z)$ be the line density perturbation at the output of the wiggler of length ℓ due to a proton at $z = s - ct = 0$. The calculation of $\delta n_\ell(z)$ has been carried out for Lorentzian energy distributions with space charge (73–76), as well as for more tightly bounded distributions (77), which yielded accurate results involving numerical integration. Results have been benchmarked against simulations (78). The effects of nonlinearities are beginning to be explored (79).

More recently, approximate formulas for a cold electron beam and no space charge were used to obtain a closed-form solution with a helical wiggler (66, 80, 81). These studies found $\delta n_\ell(z) = \hat{n}(z)\cos[kz + \phi(z)]$, where $\phi(z)$ is a slowly varying phase:

$$\hat{n}(z) = \frac{\sigma_k}{6}\exp\left[\frac{\ell}{2L} - \frac{(z - k_w\ell/3k)^2}{2\sigma_z^2}\right]. \qquad 23.$$

Here, L is the power gain length, $\sigma_k = \sigma_\omega/c$ is the FEL power bandwidth in wavenumbers, and

$$\sigma_z = \frac{2k_w\sqrt{\ell L}}{3k}, \qquad 24.$$

with $\sigma_z\sigma_k = 2/(\pi^{1/2}3^{1/4}) = 0.85738$. The power gain length satisfies $L^{-1} = 2\sqrt{3}\rho k_w$, where the FEL parameter ρ satisfies

$$(2\rho)^3 = \frac{4\pi}{\gamma k k_w A}\frac{K^2}{1 + K^2}\frac{I}{I_A}. \qquad 25.$$

Here, A is the beam area, $I_A = 17.04$ kA is the Alfvén current, $K = eB_0/(k_w m_e c)$, and the central wavenumber for a helical undulator is

$$k = k_w\frac{2\gamma^2}{1 + K^2}. \qquad 26.$$

The total perturbation at the end of the wiggler is

$$\Delta n(z) = \sum_{i=1}^{N_e} \delta n_\ell(z - z_i) + Z \sum_{i=1}^{N_I} \delta n_\ell(z - Z_i), \tag{27.}$$

where the N_e electrons in the bunch have initial coordinates z_i and the N_I ions in the bunch have initial coordinates Z_i. Being a sum of many independent random variables, $\Delta n(z)$ has a normal distribution. Taking $\sigma(\Delta n)/n = 1/M$ gives

$$\hat{n} = \frac{1}{M} \sqrt{\frac{2n_e^2}{\sqrt{\pi}\sigma_z(n_e + Z^2 n_I)}}, \tag{28.}$$

where n_e and n_I are the unperturbed densities. Setting $M = 1$ and $n_I = 0$ provides a very similar result to assuming that the saturated power of the FEL is $P_{\text{sat}} = \rho EI/e$, where E and I are the electron energy and current, respectively, and ρ is the FEL parameter (81).

After the perturbations are amplified, the electron and ion bunches are recombined. Ions create a longitudinal density perturbation, $-Ze\delta n_\ell(z)$. If the perturbation wavelength in the rest frame of the electron beam is small compared with the beam radius, one can use Gauss's law, $E_z \approx -Ze\hat{n}(z)\sin[kz + \phi(z)]/kA\epsilon_0$, where A is the cross-sectional area of the electron beam. If the wavelength in the rest frame is comparable to or larger than the beam radius, then the amplitude is reduced (80, 81). The bypass is designed so that an on-momentum particle arrives with $E_z = 0$ and off-energy particles have their energy corrected, just as in optical stochastic cooling.

Transverse cooling can be accomplished in the same way as in optical stochastic cooling or by employing magnetic elements, creating a nonzero $M_{5,1} = \partial z/\partial x$ in the electron transport between the FEL and kicker sections (65). In the latter case, the effective longitudinal field kicking the ion is $E_z \approx -Ze\hat{n}_{\max}\sin\{k[\bar{\eta}\delta + \alpha(x_\beta + D\delta)]\}/(kA\epsilon_0)$, where $x = x_\beta + D\delta$ is the offset of the proton in the kicker, $\alpha = \partial z/\partial x$ for electrons, and D is the dispersion at the kicker. The maximum perturbation $\hat{n}_{\max}$ is the smaller of Equation 27 and the peak of Equation 23. We have introduced the betatron coordinate at the kicker $x_\beta = x - D\delta$, which oscillates solely at the betatron tune. Doing so allows transverse-to-longitudinal coupling to be neglected in the calculation of the single-particle cooling rates, giving

$$\frac{\mathrm{d}\ln\hat{x}_\beta}{\mathrm{d}n} = -gD\alpha, \tag{29.}$$

$$\frac{\mathrm{d}\ln\hat{\delta}}{\mathrm{d}n} = g\bar{\eta} + gD\alpha, \tag{30.}$$

where $g = -2\pi r_c \ell_k \hat{n}_{\max}/(\gamma A)$, r_c is the classical ion radius, and ℓ_k is the effective length of the kicker section. Optimizing ℓ_k involves understanding how the plasma perturbation evolves in the kicker. For maximum kick, the perturbation reaches zero at the end of the kicker section. The plasma frequency is inversely proportional to the electron beam radius, which changes in the kicker section, although optics for focusing the electrons may be added. As with regular and optical stochastic cooling, the cooling gain is limited by multiparticle effects. The rms kick in $\Delta p/p$ is

$$\sigma(\Delta\delta) = \frac{2\pi^{5/4}\ell_k r_c}{ZkA\gamma}\sqrt{(Z^2 n_I + n_e)\hat{n}_{\max}\sigma_z}. \tag{31.}$$

This kick needs to be included in a Langevin equation for all but the lowest gains.

Recently, researchers proposed that microbunching leads to effective cooling (68). Electron and ion bunches are merged. In the modulator section, the electric field of the ion modifies the energy of nearby electrons. If we average the ion charge over a disk of radius a, then the longitudinal field

on axis from an ion is

$$E_z(z) = \frac{Ze}{2\pi\epsilon_0 a^2}\left[\frac{z}{|z|} - \frac{\gamma z}{\sqrt{\gamma^2 z^2 + a^2}}\right]. \quad 32.$$

The field acts over a distance ℓ_m, imparting $\Delta\gamma = -eE_z\ell_m/mc^2$ to the electrons. The electrons are then sent through a chicane, which can be set to either bunch or debunch the electrons. After recombination with the ions, the electrons electrostatically kick the ions. The beauty of this technique is the bunching is of a single sign so that all particles are given the correct sign of cooling. Simulations for the LHC look very promising, but as noted by Valeri Lebedev (private communication), other processes such as energy loss by coherent synchrotron radiation in the chicanes need to be considered. One must keep in mind that any change in the electron bunch length that is larger than the longitudinal slip associated with cooling will destroy cooling.

The above equations are needed to begin an estimate of cooling rates. The effects of magnetic focusing and varying beam size will modify the kick strengths. The electron bunch might be significantly shorter than the ion bunch, making the cooling dependent on the longitudinal position within the ion bunch (82, 83). There is at least one additional consideration. Bunched beam effects, especially the effect of space-charge fields, have generally been neglected. Because the relevant bunching is longitudinal, we focus on $E_{sc,z}$. If the electron and ion bunches in the comoving frame satisfy $\mathrm{d}\ln n/\mathrm{d}z \ll 1/b$, where b is the beam pipe radius, then a simple expression exists:

$$E_{sc,z}(z) \approx \frac{e}{2\pi\epsilon_0\gamma^2}\ln\left(\frac{b}{a}\right)\left[\frac{\mathrm{d}n_e}{\mathrm{d}z} - Z\frac{\mathrm{d}n_I}{\mathrm{d}z}\right]. \quad 33.$$

Equating this equation to the field of a single ion, one finds a distance $r_{sc} = \sqrt{Ze/4\pi\epsilon_0 E_{sc}}$. The equipotential surface going through this point has a radial dimension $\sim r_{sc}$. If the transverse Debye radius is larger than this value, then one might find a significant reduction in cooling.

6.2. Possibilities for eRHIC and the LHC

Coherent electron cooling systems have been proposed for the Electron RHIC (eRHIC) (60–62, 65, 66) and the LHC (61, 62, 65–68). An experimental test is currently under construction at BNL (61, 62, 66, 69, 77, 79, 84–88). The experiment will be done in the RHIC accelerator with $\gamma = 40$ gold ions. In this experiment, a 112 MHz superconducting RF (SRF) gun generates 2 MeV electron bunches. These bunches are given an energy chirp by use of 500 MHz copper cavities. After undergoing ballistic compression in a drift, they are accelerated to $\gamma = 40$ by use of a 704 MHz SRF cavity. The electron bunches are magnetically merged with the ion beam in a modulator section. Then both the ions and electrons traverse a helical wiggler. The ions, being ~4,000 times more rigid, are hardly affected, whereas the electron bunch fluctuations are amplified. The FEL instability causes the peak of the modulation produced by a given ion to travel forward by several optical wavelengths on the electron bunch. However, the electron bunch is in a wiggler, not traveling in a straight line. The net effect is that there is a limited range of wiggler parameters for which the peak density perturbation can get ahead of the ion. A chicane is then used to delay the density modulation so that its envelope peaks on the ion. Fine-tuning the delay can change cooling to anticooling, enhancing the signal-to-noise ratio of the experiment.

Table 2 shows the parameters. The rms emittance is related to the beam size via $\sigma_x(s) = \sqrt{\epsilon\beta(s)/\gamma}$, and the β function with respect to the center of the wiggler is $\beta(s) = \beta^* + s^2/\beta^*$. We take $M_{5,6} = \ell/\gamma^2$, and the value of $\hat{n}_{max}$ satisfies Equation 27 with $M = 6$. The peak cooling time within the electron bunch is 2 min, and IBS times for the gold beam are on the order of 1 h. The effects of cooling should be clearly visible.

Table 2 Coherent electron cooling parameters for an experiment at BNL and possible parameters for eRHIC

Parameter	Electron value		Ion value	
	Experiment	eRHIC	Experiment	eRHIC
Species	e^-	e^-	Au	p
Lorentz factor	42.5	260	42.5	260
Particles per bunch	6×10^{10}	6×10^{10}	10^9	2×10^{11}
Peak current	77 A	77 A	5 A	50 A
rms emittance, ϵ	5 μm	1 μm	2 μm	1 μm
rms, δ	5×10^{-4}	1×10^{-3}	1×10^{-3}	1×10^{-3}
Modulator length	3 m	9 m	NA	NA
Kicker length	3 m	9 m	NA	NA
β^*	3.75 m	3.75 m	NA	NA
FEL length	7.5 m	7.5 m	NA	NA
λ_w	4 cm	3 cm	NA	NA
λ	13.8 μm	0.44 μm	NA	NA
K	0.5	1	NA	NA
$\hat{n}_{\max}$	1.5×10^7 m^{-1}	2.0×10^8 m^{-1}	NA	NA
One-dimensional cooling time	2 min	8 min	NA	NA

Adapted (roughly) from Reference 66. Abbreviations: FEL, free electron laser; NA, not applicable; rms, root mean square.

Table 2 also shows some possible parameters for eRHIC. The value $\bar{\eta} = 7.0 \times 10^{-5}$ m was obtained from the assumption that $k\bar{\eta}\sigma(\delta) = 1$ with $\sigma(\delta) = 10^{-3}$. Equation 30 is satisfied with $M \approx 2.5$. Although the details of eRHIC are unclear, such a system would probably improve performance. Estimates for the LHC are complicated by the fact that the density perturbations in the rest frame of the bunch are likely to be longer than the bunch radius, and no estimate will be attempted. Existing estimates show little benefit (81).

7. SUMMARY AND CONCLUSIONS

This article reviews cooling techniques for high-energy hadron beams. Stochastic cooling is effective for the small particle densities found in heavy-ion beams and can provide useful cooling at moderate cost. Accurate simulations are available, and there is little risk. Electron cooling has been proposed for 150 GeV protons and may be useful in an electron–ion collider. The two techniques that are most likely to benefit high-energy proton beams are optical stochastic cooling and coherent electron cooling. Optical stochastic cooling may benefit the LHC but would be difficult in RHIC and eRHIC owing to the necessary energy scans. Coherent electron cooling holds much promise for our field, but the challenges are significant. The BNL experiment will answer many questions, but more theory and simulations are clearly warranted. The influence of space-charge forces within the modulator is a relevant topic. Although it may turn out to be a nonissue, it is likely that some important effects have not been studied—all the more reason to push forward with experimental tests.

DISCLOSURE STATEMENT

The author is not aware of any affiliations, memberships, funding, or financial holdings that might be perceived as affecting the objectivity of this review.

ACKNOWLEDGMENTS

This work has benefited from conversations with several people. It is my pleasure to thank Mike Brennan, Fritz Caspers, Alexei Fedotov, Wolfram Fischer, John Jowett, Valeri Lebedev, Vladimir Litvinenko, Dave McGinnis, Ralph Pasquinelli, Thomas Roser, Michaela Schaumann, Gang Wang, Sasha Zholents, and Max Zolotorev.

LITERATURE CITED

1. Piwinski A. In *Handbook of Accelerator Physics and Engineering*, ed. AW Chao, M Tigner, p. 125. Singapore: World Sci. 1st ed. (1999)
2. Chao AW, Mess KH, Tigner M, Zimmermann F, ed. *Handbook of Accelerator Physics and Engineering.* Singapore: World Sci. 2nd ed. (2013)
3. Sorensen AH. *Lect. Notes Phys.* 400:467 (1992)
4. Van der Meer S. *Rev. Mod. Phys.* 57:689 (1985)
5. Mohl D. In *Internal Note 87-03*, ed. S Turner, p. 453. Geneva: CERN (1987)
6. Herr H, Mohl D. *Proc. Workshop Phase Space Cool. High Energy Beams*, p. 41. Madison: Univ. Wis. Press (1978)
7. Sacherer F. *Internal Note CERN-ISR-TH/78-11*. Geneva: CERN (1978)
8. Chattopadhyay S. *On stochastic cooling of bunched beams from fluctuation and kinetic theory*. PhD thesis LBL-14826, Univ. Calif., Berkeley. 286 pp. (1982)
9. Chattopadhyay S. *IEEE Trans. Nucl. Sci.* 30:2646 (1983)
10. Chattopadhyay S. *IEEE Trans. Nucl. Sci.* 30:2649 (1983)
11. Chattopadhyay S. *IEEE Trans. Nucl. Sci.* 30:2334 (1983)
12. Boussard D, Chattopadhyay S, Dome G, Linnecar T. In *Internal Note 84-15*, ed. P Bryant, S Newman, p. 197. Geneva: CERN (1984)
13. Jackson G. *Proc. 1991 Part. Accel. Conf.* (*PAC1991*), p. 2532. Piscataway, NJ: IEEE (1991)
14. Boussard D. *Lect. Notes Phys.* 296:289 (1986)
15. Jackson G, et al. *Proc. Workshop Adv. Beam Instrum.*, p. 312. Tsukuba, Jpn.: KEK (1991)
16. Caspers F, Mohl D. *Proc. 17th Int. Conf. High Energy Accel.*, p. 297. Dubna, Russ.: Jt. Inst. Nucl. Res. (1999)
17. Jackson G. *Proc. 1993 Workshop Beam Cool. Relat. Top.*, p. 127. Geneva: CERN (1994)
18. Pasquinelli RJ. *Proc. 1995 Part. Accel. Conf.* (*PAC1905*), p. 2379. Piscataway, NJ: IEEE (1995)
19. Van der Meer S. *Internal Note RHIC-AP-9*. Upton, NY: Brookhaven Natl. Lab. (1984)
20. Wei J, Ruggiero AG. *Internal Note BNL/AD/RHIC-71.* Upton, NY: Brookhaven Natl. Lab. (1990)
21. Blaskiewicz M, Brennan JM, *Proc. 2005 Part. Accel. Conf.* (*PAC2005*), p. 310. Piscataway, NJ: IEEE (2005)
22. Blaskiewicz M, Brennan JM. *Phys. Rev. Spec. Top. Accel. Beams* 10:061001 (2007)
23. Blaskiewicz M, Brennan JM. *Proc. 2007 Workshop Beam Cool. Relat. Top.* (*COOL2007*), p. 125. Darmstadt, Ger.: DSI (2007)
24. Carron G, Thorndahl L. *Internal Note CERN-ISR-RF/78-12*. Geneva: CERN (1978)
25. Blaskiewicz M, Brennan JM, Mernick K. *Proc. 2013 Workshop Beam Cool. Relat. Top.* (*COOL2013*), p. 6. JACoW.org: Jt. Accel. Conf. Website (2013)
26. Mernick K, et al. *Proc. 14th Beam Instrum. Workshop* (*BIW10*), p. 389. JACoW.org: Jt. Accel. Conf. Website (2010)
27. McGinnis D, et al. *Proc. 1991 Part. Accel. Conf.* (*PAC1991*), p. 1389. Piscataway, NJ: IEEE (1991)
28. Schaumann M, Jowett JM, Blaskiewicz M. *Proc. 2013 Workshop Beam Cool. Relat. Top.* (*COOL2013*), p. 76. JACoW.org: Jt. Accel. Conf. Website (2013)
29. Budker GI. *At. Energ.* 22:346 (1967)
30. Sorensen AH, Bonderup E. *Nucl. Instrum. Methods* 215:27 (1983)
31. Poth H. *Phys. Rep.* 196:135 (1990)
32. Chandrasekhar S. *Astron. Phys. J.* 97:255 (1943)
33. Derbenev YS, Skrinsky AN. *Part. Accel.* 8:1 (1977)

34. Burov A, et al. *Phys. Rev. Spec. Top. Accel. Beams* 3:094002 (2000)
35. Sidorin AO, et al. *Nucl. Instrum. Methods A* 588:325 (2006)
36. Nagaitsev S, et al. *Phys. Rev. Lett.* 96:044801 (2006)
37. Fedotov AV, et al. *Phys. Rev. Spec. Top. Accel. Beams* 9:074401 (2006)
38. Ben-Zvi I, et al. *Nucl. Instrum. Methods A* 532:177 (2004)
39. Fedotov AV, et al. *New J. Phys.* 8:283 (2006)
40. Fedotov AV, et al. *Phys. Rev. Spec. Top. Accel. Beams* 9:074401 (2006)
41. Fedotov AV, et al. *Phys. Rev. E* 73:066503 (2006)
42. Ben-Zvi I. *Proc. 2006 Eur. Part. Accel. Conf.* (*EPAC2006*), p. 940. Geneva: Eur. Phys. Soc. Accel. Group (2006)
43. Derbenev YS, et al. *Proc. 2012 ICFA Adv. Beam Dyn. Workshop* (*HB2012*), p. 219. JACoW.org: Jt. Accel. Conf. Website (2012)
44. Zhang Y, Bisognano J, ed. arXiv:1209.0757 [physics] (2012)
45. Derbenev YS, Zhang Y. *Proc. 2009 Workshop Beam Cool. Relat. Top.* (*COOL2009*), p. 181. Lanzhou, China: Inst. Mod. Phys. (2009)
46. Mikhailichenko AA, Zoltorev MS. *Phys. Rev. Lett.* 71:4146 (1993)
47. Zoltorev MS, Zholents AA. *Phys. Rev. E* 50:3087 (1994)
48. Lebedev V. *Proc. 2010 ICFA Adv. Beam Dyn. Workshop* (*HB2010*), p. 644. JACoW.org: Jt. Accel. Conf. Website (2010)
49. Murphy JB, Pellegrini C. In *Laser Handbook*, Vol. 6, p. 9. Amsterdam: North Holland (1990)
50. Boyd GD, Gordon JP. *Bell Syst. Technol. J.* 40:489 (1961)
51. Bessonov EG, Gorbunkov MV, Mikhailichenko AA. *Proc. 2006 Eur. Part. Accel. Conf.* (*EPAC2006*), p. 1483. Geneva: Eur. Phys. Soc. Accel. Group (2006)
52. Bessonov EG, Gorbunkov MV, Mikhailichenko AA. *Phys. Rev. Spec. Top. Accel. Beams* 11:011302 (2008)
53. Babzien M, et al. *Phys. Rev. Spec. Top. Accel. Beams* 7:012801 (20014)
54. Lebedev V, Zolotorev MS. *Proc. 2012 ICFA Adv. Beam Dyn. Workshop* (*HB2012*), p. 514. JACoW.org: Jt. Accel. Conf. Website (2012)
55. Franklin W, et al. *Proc. 2007 Workshop Beam Cool. Relat. Top.* (*COOL2007*), p. 117. Darmstadt, Ger.: DSI (2007)
56. Lebedev VA, Tokpanov Y, Zolotorev MS. *Proc. 2013 N. Am. Part. Accel. Conf.* (NA-*PAC13*), p. 442. JACoW.org: Jt. Accel. Conf. Website (2013)
57. Moulton PF. *J. Opt. Soc. Am. B* 1:125 (1986)
58. Cerullo G, De Silvestri S. *Rev. Sci. Instrum.* 74:1 (2003)
59. Derbenev YS. *AIP Conf. Proc.* 253:103 (1992)
60. Litvinenko VL, Derbenev YS. *Phys. Rev. Lett.* 102:114801 (2009)
61. Litvinenko VL, Derbenev YS. *Proc. 2007 Int. Free Electron Laser Conf.* (*FEL2007*), p. 268. Novosibirsk, Russ.: Budker Inst. Nucl. Phys. (2007)
62. Litvinenko VL, Derbenev YS. *Proc. 2008 Eur. Part. Accel. Conf.* (*EPAC2008*), p. 1560. Geneva: Eur. Phys. Soc. Accel. Group (2008)
63. Bell GI, et al. *Proc. 2008 Eur. Part. Accel. Conf.* (*EPAC2008*), p. 3185. Geneva: Eur. Phys. Soc. Accel. Group (2008)
64. Wang G, Blaskiewicz M. *Phys. Rev. E* 78:026413 (2008)
65. Litvinenko VL. *Proc. 2009 Part. Accel. Conf.* (*PAC2009*), p. 4236. Piscataway, NJ: IEEE (2009)
66. Litvinenko VL. *Proc. 2013 Workshop Beam Cool. Relat. Top.* (*COOL2013*), p. 175. JACoW.org: Jt. Accel. Conf. Website (2013)
67. Elizarov A, Litvinenko V. *Phys. Rev. Spec. Top. Accel. Beams* 16:124001 (2013)
68. Ratner D. *Phys. Rev. Lett.* 111:084802 (2013)
69. Schwartz BT, et al. *Proc. 4th Int. Part. Accel. Conf.* (*IPAC2013*), p. 1049. Piscataway, NJ: IEEE (2013)
70. Bell G, et al. *Proc. 2011 Part. Accel. Conf.* (*PAC2011*), p. 235. Piscataway, NJ: IEEE (2011)
71. Wang G, Blaskiewicz M, Litvinenko VN. *Proc. 1st Int. Part. Accel. Conf.* (*IPAC2010*), p. 873. Piscataway, NJ: IEEE (2010)
72. Elizarov A, Litvinenko VN. *Proc. 4th Int. Part. Accel. Conf.* (*IPAC2013*), p. 1082. Piscataway, NJ: IEEE (2013)

73. Wang G, Blaskiewicz M, Litvinenko VL. *Proc. 2009 Part. Accel. Conf.* (*PAC2009*), p. 1460. Piscataway, NJ: IEEE (2009)
74. Wang G. *Coherent electron cooling and two stream instabilities due to coherent elecron cooling*. PhD thesis, State Univ. N.Y., Stony Brook. 142 pp. (2008)
75. Wang G, Litvinenko VN, Blaskiewicz M. *Proc. 4th Int. Part. Accel. Conf.* (*IPAC2013*), p. 276. Piscataway, NJ: IEEE (2013)
76. Bell G, et al. *Proc. 3rd Int. Part. Accel. Conf.* (*IPAC2012*), p. 3231. Piscataway, NJ: IEEE (2012)
77. Wang G, Hao Y, Litvinenko VN, Webb SD. *Proc. 3rd Int. Part. Accel. Conf.* (*IPAC2012*), p. 3213. Piscataway, NJ: IEEE (2012)
78. Hao Y, Litvinenko VN. *Proc. 3rd Int. Part. Accel. Conf.* (*IPAC2012*), p. 448. Piscataway, NJ: IEEE (2012)
79. Elizarov A, Litvinenko VN. *Proc. 2012 Int. Free Electron Laser Conf.* (*FEL2012*), p. 77. JACoW.org: Jt. Accel. Conf. Website (2012)
80. Stupakov G, Zolotorev MS. *Phys. Rev. Lett.* 110:269503 (2013)
81. Stupakov G, Zolotorev MS. *Proc. 2013 Int. Free Electron Laser Conf.* (*FEL2013*), p. 132. JACoW.org: Jt. Accel. Conf. Website (2013)
82. Webb S, Wang G, Litvinenko VN. *Proc. 2011 Part. Accel. Conf.* (*PAC2011*), p. 232. Piscataway, NJ: IEEE (2011)
83. Webb S. *Theoretical considerations for coherent electron cooling*. PhD thesis, State Univ. N.Y., Stony Brook. 111 pp. (2011)
84. Litvinenko VN, et al. *Proc. 2nd Int. Part. Accel. Conf.* (*IPAC2011*), p. 3442. Piscataway, NJ: IEEE (2011)
85. Pinayev I, et al. *Proc. 3rd Int. Part. Accel. Conf.* (*IPAC2012*), p. 400. Piscataway, NJ: IEEE (2012)
86. Pinayev I, et al. *Proc. 4th Int. Part. Accel. Conf.* (*IPAC2013*), p. 1535. Piscataway, NJ: IEEE (2013)
87. Gassner DM, et al. *Proc. 15th Beam Instrum. Workshop* (*BIW12*), p. 231. JACoW.org: Jt. Accel. Conf. Website (2012)
88. Pinayev I, et al. *Proc. 2013 Workshop Beam Cool. Relat. Top.* (*COOL2013*), p. 127. JACoW.org: Jt. Accel. Conf. Website (2013)